PERGAMON

International Journal of Solids and Structures 37 (2000) 7161–7183

INTERNATIONAL JOURNAL OF SOLIDS and STRUCTURES

www.elsevier.com/locate/ijsolstr

Modeling fracture in Mindlin–Reissner plates with the extended finite element method

John Dolbow [a,*], Nicolas Moës [b], Ted Belytschko [b]

[a] *Department of Civil and Environmental Engineering, Duke University, Box 90287 Durham, NC 27708-0287, USA*
[b] *Department of Mechanical Engineering, Northwestern University, Evanston, IL 60208, USA*

Received 1 September 1999; in revised form 20 January 2000

Abstract

A technique for the modeling of cracks and crack growth in plates using the extended finite element method (X-FEM) is presented. Beginning with a plate formulation which does not exhibit shear locking, the finite element approximation is enriched with both discontinuous and near-tip functions. This allows for the modeling of crack geometries which are independent of the finite element mesh topology, and greatly facilitates the simulation of crack growth. Guidelines for the construction of the enriched approximation and the numerical integration of the weak form in the X-FEM framework are reviewed. To obtain the mixed-mode stress intensity factors, we derive appropriate domain forms of an interaction integral in the context of Mindlin–Reissner plate theory. Several benchmark problems of through-the-thickness cracks in infinite and finite plates are solved to illustrate the accuracy and utility of the new formulation.

Keywords: Modeling fracture; Crack growth; Shear locking

1. Introduction

Plate and shell formulations are widely used to analyze thin-walled structures such as aircraft fuselages subjected to bending and pressure loads. Through-the-thickness cracks (often called through cracks) may develop when these structures are subjected to cyclic loads, and the determination of mixed-mode stress intensity factors is critical to the modeling of fatigue crack propagation. Despite the practical importance, relatively little research has focused on developing robust numerical methods to determine fracture parameters and simulate crack growth in thin plates. Standard finite element formulations for crack growth are burdened by the need to remesh at each stage of crack evolution, as well as uncertainties in the use of path-independent integrals to calculate shear and moment intensity factors. In this paper, we address both difficulties by developing a suitable domain form of the interaction integral in conjunction with the extended finite element method (X-FEM) to model the fracture of Mindlin–Reissner plates.

* Corresponding author. Fax: +1-919-660-5219.
E-mail address: jdolbow@duke.edu (J. Dolbow).

0020-7683/00/$ - see front matter
PII: S0020-7683(00)00194-3

The Mindlin–Reissner plate theory is attractive for the numerical simulation of fracture for several reasons. In comparison to the Kirchhoff theory, the Mindlin–Reissner theory allows for transverse shear strains through the thickness of the plate. This in turn enables the three boundary conditions at the free surface of the crack face to be met, and results in an angular distribution of stresses consistent with the three-dimensional theory at the crack tip (Knowles and Wang, 1960). With regards to finite element discretization, the Mindlin–Reissner variational formulation places fewer restrictions on the smoothness of the approximating space, so that the plate displacements can be approximated with classical C^0 interpolations. Despite these advantages, finite element formulations based on Mindlin–Reissner theory for fracture analysis are complicated by shear-locking and the calculation of mixed-mode intensity factors.

Analogous to the stress intensity factors of classical three-dimensional fracture mechanics, in Mindlin–Reissner theory the near-tip fields are described in terms of moment and shear force intensity factors. The definition of these quantities can be found in Sih (1977), with analytical solutions for some simple geometries. Unfortunately, many of these solutions were recently shown to be incorrect for thin plates (Joseph and Erdogan, 1991). More recent analytical and numerical results are limited to simple geometries, and quite often are only available for pure Mode I loadings. One reason for the latter is the apparent lack of a suitable method to extract the mixed-mode intensity factors. While some work has been performed in this area (Sosa and Herrmann, 1989; Sosa and Eischen, 1986), the derived contour integrals are not well suited to finite element calculations, and in some cases only accomplish part of the task. The issue is addressed in the present paper by developing a domain form of the interaction integral.

When considering finite element approximations of relatively thin plates, it is necessary to address the phenomenon known as shear locking. As the plate becomes very thin, both the solution and its approximation must satisfy the constraint that the transverse shear strains vanish in the domain. When there are not enough functions in the finite element subspace which satisfy this constraint, a poor approximation results for the plate displacements. Fortunately, plate elements have been developed which do not exhibit shear locking. See Pitkäranta and Suri (1996) for an excellent review of several plate elements and the pertinent issues. Concerning the modeling of fracture, the free surface of the crack faces presents additional challenges, and some elements perform much better than others (Pitkäranta and Suri, 2000). Numerical studies of plate fracture often use less robust formulations, and examine only relatively thick plates. In the present investigation, we examine the performance of the MITC4 element (Bathe, 1996) in fracture analysis.

A limited amount of research has focused on the simulation of crack growth in Mindlin–Reissner plates. Crack growth in thin shells was simulated with finite elements and continuous remeshing in Potyondy et al. (1995), in which the growth direction was determined using stress intensity factors obtained from a fracture analysis of the Kirchhoff model for thin plates (Hui and Zehnder, 1993). The X-FEM has recently emerged as a promising alternative to model crack growth with finite elements without the need to remesh the domain. The present technique has a distinct advantage over boundary element methods as it is readily applicable to non-linear problems, anisotropic materials, and arbitrary geometries. The method originates to Belytschko and Black (1999), where a standard two-dimensional finite element approximation was enriched with the asymptotic near-tip fields. By aligning the discontinuity in the near-tip fields with the crack, a crack geometry which is independent of the finite element mesh was modeled. This formulation was extended in Moës et al. (1999) by replacing the near-tip functions with a simple discontinuous function away from the crack tip. In addition to fracture mechanics, the method has been generalized and applied to other problems in applied mechanics (Dolbow et al., 2000; Dolbow, 1999).

The key concept behind the X-FEM is the incorporation of special enrichment functions into a standard finite element approximation. The enriched approximation is constructed using the partition of unity concept (Melenk and Babuška, 1996; Duarte and Oden, 1995). In this framework, global enrichment functions are multiplied by the local finite element partition of unity. This construct ensures a conforming approximation and retains a measure of sparsity in the discrete equations. A key feature of the X-FEM is the use of discontinuous enrichment functions and modified integration algorithms to construct the stiffness

matrix. These allow the method to model geometric features which are topologically independent of the finite element mesh.

This paper is organized as follows. In the next section, we summarize the governing equations and variational formulation for the fracture of Mindlin–Reissner plates. Section 3 describes the discrete approximation in the X-FEM framework. In order to extract the mixed-mode intensity factors, a domain form of the interaction integral for plates is derived in Section 4. Numerical examples are given in Section 5, and some concluding remarks are provided in Section 6.

2. Problem formulation

There are several different ways to introduce the Mindlin theory. In this section, the governing equations are developed from the integration of the principle of virtual work through the thickness with the appropriate kinematic assumptions.

2.1. Governing equations

Consider the domain $\Omega \subset \mathscr{R}^2$ with boundary Γ which represents the mid-plane of a plate with thickness t occupying the region $\Omega \times (-t/2, t/2)$. We designate Γ_d as an internal surface across which the displacement field may be discontinuous. The conventions adopted in this paper are shown in Fig. 1. The main assumptions of the Mindlin theory state that the in plane displacements, u_1 and u_2 vary linearly through the thickness with the section rotations ψ_1 and ψ_2. In addition, the normal stress σ_{33} is assumed to vanish in the domain. We make the additional assumptions that the surfaces of the plate ($x_3 = t/2, -t/2$) and any crack faces are traction-free.

In the $(\boldsymbol{e}_1, \boldsymbol{e}_2, \boldsymbol{e}_3)$ basis, where $\boldsymbol{e}_3$ is the unit normal vector to the plate, the displacement components at a point (x_1, x_2, x_3) are given by

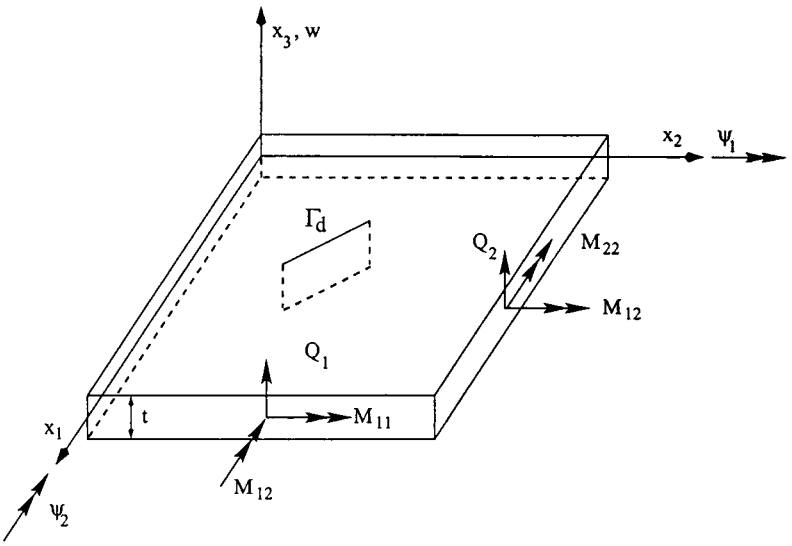

Fig. 1. Notations and sign conventions for a plate with a through crack.

$$\boldsymbol{u}(\boldsymbol{x}) = \begin{cases} u_1 = x_3\psi_1(x_1, x_2), \\ u_2 = x_3\psi_2(x_1, x_2), \\ u_3 = w(x_1, x_2), \end{cases} \tag{1}$$

where w is the transverse displacement and ψ_1 and ψ_2 are section rotations about the x_2 and x_1 axes, respectively. The above can be expressed in a more compact form as

$$\boldsymbol{u}(\boldsymbol{x}) = w\boldsymbol{e}_3 + x_3\boldsymbol{\psi}, \tag{2}$$

where $\boldsymbol{\psi} = \psi_1\boldsymbol{e}_1 + \psi_2\boldsymbol{e}_2$.

The strain is given by

$$\tfrac{1}{2}(\nabla\boldsymbol{u} + (\nabla\boldsymbol{u})^t) = x_3\boldsymbol{\epsilon}_{\mathrm{b}}(\boldsymbol{\psi}) + \tfrac{1}{2}(\boldsymbol{\epsilon}_{\mathrm{s}}(w, \boldsymbol{\psi}) \otimes \boldsymbol{e}_3 + \boldsymbol{e}_3 \otimes \boldsymbol{\epsilon}_{\mathrm{s}}(w, \boldsymbol{\psi})) \tag{3}$$

with the bending contribution

$$\boldsymbol{\epsilon}_{\mathrm{b}}(\boldsymbol{\psi}) = \tfrac{1}{2}\big(\nabla\boldsymbol{\psi} + (\nabla\boldsymbol{\psi})^t\big) \tag{4}$$

and a shear contribution

$$\boldsymbol{\epsilon}_{\mathrm{s}}(w, \boldsymbol{\psi}) = \nabla w + \boldsymbol{\psi}. \tag{5}$$

We note that the $\boldsymbol{e}_3$ related components are zero for both $\boldsymbol{\epsilon}_{\mathrm{b}}$ and $\boldsymbol{\epsilon}_{\mathrm{s}}$.

The virtual internal work is defined by

$$\delta W^{\mathrm{int}} = \int_{\Omega} \boldsymbol{\sigma} : \nabla(\delta\mathbf{u})\mathrm{d}\Omega, \tag{6}$$

where $\boldsymbol{\sigma}$ is the symmetric stress tensor, and $\delta\mathbf{u}$ is an arbitrary virtual displacement from the current position. After a few manipulations, we obtain the relation

$$\boldsymbol{\sigma} : \nabla(\delta\mathbf{u}) = x_3\boldsymbol{\sigma}^{\pi} : \boldsymbol{\epsilon}_{\mathrm{b}}(\delta\boldsymbol{\psi}) + \boldsymbol{\sigma}^{\mathrm{s}} \cdot \boldsymbol{\epsilon}_{\mathrm{s}}(\delta w, \delta\boldsymbol{\psi}), \tag{7}$$

where the π superscript indicates a reduction of the operator to the in plane $(\boldsymbol{e}_1, \boldsymbol{e}_2)$ components and $\boldsymbol{\sigma}^{\mathrm{s}}$ is the shear stress vector $\boldsymbol{\sigma}^{\mathrm{s}} = \boldsymbol{\sigma} \cdot \boldsymbol{e}_3$.

Substituting Eq. (7) into Eq. (6) and integrating through the thickness gives the work expression

$$\delta W^{\mathrm{int}} = \int_{\Omega} (\boldsymbol{M} : \boldsymbol{\epsilon}_{\mathrm{b}}(\boldsymbol{\psi}) + \boldsymbol{Q} \cdot \boldsymbol{\epsilon}_{\mathrm{s}}(w, \boldsymbol{\psi}))\mathrm{d}\Omega, \tag{8}$$

where the moment $\boldsymbol{M}$ and shear $\boldsymbol{Q}$ are defined by

$$\boldsymbol{M} = \int_{-t/2}^{t/2} x_3\boldsymbol{\sigma}^{\pi}\mathrm{d}x_3, \qquad \boldsymbol{Q} = \int_{-t/2}^{t/2} \boldsymbol{\sigma}^{\mathrm{s}}\mathrm{d}x_3. \tag{9}$$

The virtual external work is composed of the action of the bending and twisting moments gathered in a couple vector $\boldsymbol{C}$, and of the shear traction T. As previously stated, we assume there is no external pressure acting on the plate. The virtual external work is then

$$\delta W^{\mathrm{ext}} = \int_{\Gamma} \boldsymbol{C} \cdot \delta\boldsymbol{\psi}\,\mathrm{d}\Gamma + \int_{\Gamma} T\delta w\,\mathrm{d}\Gamma. \tag{10}$$

Equating the internal and external virtual work, and applying the divergence theorem yields the equilibrium equations in Ω

$$\nabla \cdot \boldsymbol{M} - \boldsymbol{Q} = 0 \tag{11a}$$

$$\nabla \cdot \boldsymbol{Q} = 0 \tag{11b}$$

and the traction boundary conditions on Γ

$$\boldsymbol{C} = \boldsymbol{M} \cdot \boldsymbol{n}, \tag{12a}$$

$$T = \boldsymbol{Q} \cdot \boldsymbol{n}, \tag{12b}$$

where $\boldsymbol{n}$ is the unit outward normal to the boundary.

The constitutive relationships are obtained by energetic equivalence between the plate and the three-dimensional model. Assuming the plate is made of an isotropic homogeneous elastic material of Young's modulus E and of Poisson's ratio v, the constitutive relations are given by

$$\begin{bmatrix} M_{11} \\ M_{22} \\ M_{12} \end{bmatrix} = \frac{Et^3}{12(1-v^2)} \begin{bmatrix} 1 & v & 0 \\ v & 1 & 0 \\ 0 & 0 & 1-v \end{bmatrix} \begin{bmatrix} \epsilon_{\mathrm{b}11} \\ \epsilon_{\mathrm{b}22} \\ \epsilon_{\mathrm{b}12} \end{bmatrix} \tag{13}$$

and

$$\begin{bmatrix} Q_1 \\ Q_2 \end{bmatrix} = \mu k t \begin{bmatrix} \epsilon_{\mathrm{s}1} \\ \epsilon_{\mathrm{s}2} \end{bmatrix}, \tag{14}$$

where μ is the shear modulus. The correction factor k accounts for the parabolic variation of the transverse shear stresses through the thickness of the plate, and is taken to be $k = 5/6$.

The above equations can be rewritten in a more compact form using the fourth order bending stiffness tensor $\boldsymbol{D}_{\mathrm{b}}$ and the second order shear stiffness tensor $\boldsymbol{D}_{\mathrm{s}}$:

$$\boldsymbol{M} = \boldsymbol{D}_{\mathrm{b}} \boldsymbol{\epsilon}_{\mathrm{b}}, \qquad \boldsymbol{Q} = \boldsymbol{D}_{\mathrm{s}} \boldsymbol{\epsilon}_{\mathrm{s}}. \tag{15}$$

2.2. Variational formulation

Let the boundary Γ be divided into a part Γ_u on which kinematic boundary conditions $(w_g, \boldsymbol{\psi}_g)$ are imposed and a part Γ_t on which loads are applied with the restrictions

$$\Gamma = \Gamma_u \cup \Gamma_t \quad \Gamma_u \cap \Gamma_t = \emptyset. \tag{16}$$

The kinematics constraints are given by a prescribed transverse displacement w and prescribed rotations $\boldsymbol{\psi}$ while the loads come from the prescribed couples $\boldsymbol{C}$ and prescribed shear tractions T.

Let $\mathscr{U}$ be the space of kinematically admissible transverse displacements and rotations

$$\mathscr{U} = \{(w, \boldsymbol{\psi}) \in \mathscr{V} : w = w_g, \boldsymbol{\psi} = \boldsymbol{\psi}_g \quad \text{on } \Gamma_u\}, \tag{17}$$

where $\mathscr{V}$ is a space of sufficiently smooth functions on Ω. The details on the regularity of the space are discussed in Babuška and Rosenzweig (1972) and Grisvard (1985). We note that the space $\mathscr{V}$ allows for discontinuous functions across Γ_{d}.

The space of test functions is defined similarly as

$$\mathscr{U}_0 = \{(w, \boldsymbol{\psi}) \in \mathscr{V} : w = 0, \boldsymbol{\psi} = 0 \quad \text{on } \Gamma_u\}. \tag{18}$$

The weak form is to find $(w, \boldsymbol{\psi}) \in \mathscr{U}$ such that

$$\int_\Omega (\boldsymbol{D}_{\mathrm{b}} \boldsymbol{\epsilon}_{\mathrm{b}}(\boldsymbol{\psi})) : \boldsymbol{\epsilon}_{\mathrm{b}}(\delta\boldsymbol{\psi}) \mathrm{d}\Omega + \int_\Omega (\boldsymbol{D}_{\mathrm{s}} \boldsymbol{\epsilon}_{\mathrm{s}}(w, \boldsymbol{\psi})) \cdot \boldsymbol{\epsilon}_{\mathrm{s}}(\delta w, \delta\boldsymbol{\psi}) \mathrm{d}\Omega$$
$$= \int_\Gamma \boldsymbol{C} \cdot \delta\boldsymbol{\psi} \, \mathrm{d}\Gamma + \int_\Gamma T \delta w \, \mathrm{d}\Gamma \quad \forall (\delta w, \delta\boldsymbol{\psi}) \in \mathscr{U}_0. \tag{19}$$

It can be shown that the above is equivalent to the equilibrium equations (11a) and (11b) and traction boundary conditions (12a) and (12b). When the space $\mathscr{V}$ is discontinuous along Γ_{d}, the traction-free conditions on the crack faces are also satisfied.

3. Extended finite element approximation

In this section, we present the methodology of constructing a discrete approximation to the plate displacements with the X-FEM. The essential concept behind the X-FEM is the modeling of geometric features which are independent of the topology of the finite element mesh. This is effected through the implementation of enrichment functions and modifications to the integration of the weak form. Only the essential details are provided in this section, see Moës et al. (1999) or Dolbow (1999) for more details.

In the following, we first describe a standard plate approximation which does not exhibit shear locking. The manner in which this formulation is enriched with both discontinuous and near-tip fields in the X-FEM framework is then described. Finally, modifications made to the numerical integration of the Galerkin weak form are discussed.

3.1. Discretization with the MITC4 plate element

When discretizing the plate equations (11a) and (11b), some care must be taken for thin plates. As the plate becomes very thin, the following relationship must be satisfied to keep the strain energy in the plate bounded

$$\nabla w + \boldsymbol{\psi} = 0. \tag{20}$$

In other words, the shear strain $\boldsymbol{\epsilon}_s$ must vanish in the domain as $t \to 0$. This condition is known as the Kirchhoff constraint, and it applies to both the solution $(w, \boldsymbol{\psi})$ and its approximation $(w^h, \boldsymbol{\psi}^h)$. When there are not enough functions in $\mathscr{V}^h$ which satisfy Eq. (20), a degradation in the accuracy and initial rates of convergence is observed for the plate displacements $(w^h, \boldsymbol{\psi}^h)$. This phenomenon is often referred to as shear locking.

Several different element formulations have been developed to address the shear locking issue. A consideration when dealing with plate fracture is the element performance near the free surface of the crack faces, and in this regard the MITC class of elements (Bathe et al., 1990) offer superior performance over other available formulations (see the analysis of Pitkäranta and Suri, 1996). In the following, we review only the standard approximation.

Following Brezzi et al. (1989), we denote the admissible spaces of rotations and transverse displacement by $\boldsymbol{\Psi}$ and $\mathscr{W}$, respectively. When the domain does not contain an internal boundary or re-entrant corner, these are usually taken to be $\boldsymbol{\Psi} = (H_0^1(\Omega))^2$ and $\mathscr{W} = H_0^1(\Omega)$. The finite element subspaces are then denoted by $\boldsymbol{\Psi}^h \subset \boldsymbol{\Psi}$ and $\mathscr{W}^h \subset \mathscr{W}$.

Consider the specific approximations $\boldsymbol{\psi}^h \in \boldsymbol{\Psi}^h$ and $w^h \in \mathscr{W}^h$. The MITC formulation avoids shear locking by making a modification to the expression for the shear energy

$$\mu k t ||\boldsymbol{\psi}^h - \nabla w^h||_0^2 \tag{21}$$

by applying a bounded linear operator R with values in a third space Γ^h. This operator is applied to the shear energy as

$$\mu k t ||R\boldsymbol{\psi}^h - \nabla w^h||_0^2. \tag{22}$$

The choice of this reduction operator, in conjunction with the spaces $\boldsymbol{\Psi}^h$, $\mathscr{W}^h$, and Γ^h is not arbitrary. Brezzi et al. (1989) outline a set of five criteria for these spaces to satisfy in order to maintain convergence.

In the present investigation, we consider only the MITC4 element, whose approximation is based on the 4-node isoparametric quadrilateral. The resulting formulation is identical to that developed in Hughes and Tezduyar (1981). Let us assume that we have a triangulation of the domain Ω and that each element is a quadrilateral. Each element E is the image of a reference quadrilateral $\hat{E}$ through an invertible mapping:

$\boldsymbol{x} = \boldsymbol{x}(\boldsymbol{\xi})\ \boldsymbol{\xi} \in [-1,1] \times [-1,1]$. On each element the transverse displacement field is expressed in terms of the four nodal coefficients $w_i, i = 1, \ldots 4$ through the classical bilinear shape functions ϕ_i

$$w^h(\boldsymbol{x}) = \sum_{i=1}^{4} \phi_i(\boldsymbol{\xi}(\boldsymbol{x}))w_i, \qquad \boldsymbol{x} \in E, \quad \boldsymbol{\xi} \in \hat{E}. \tag{23}$$

The rotation field in the bending term (the first term in Eq. (19)) also uses the classical bilinear shape functions; the degrees of freedom being the $\boldsymbol{e}_1$ and $\boldsymbol{e}_2$ components of the vector $\boldsymbol{\psi}$ at each of the four nodes of the element

$$\boldsymbol{\psi}(\boldsymbol{x}) = \sum_{i=1}^{4} \phi_i(\boldsymbol{\xi}(\boldsymbol{x}))\boldsymbol{\psi}_i, \qquad \boldsymbol{x} \in E, \quad \boldsymbol{\xi} \in \hat{E}. \tag{24}$$

The reduction operator R is implemented by modifying the approximation of the rotation vector in the shear term (second term in Eq. (19)). We express this modification through the special shape functions $\tilde{\boldsymbol{\phi}}_i$ as

$$\boldsymbol{\psi}(\boldsymbol{x}) = \sum_{i=1}^{4} \tilde{\boldsymbol{\phi}}_i(\boldsymbol{\xi}(\boldsymbol{x}))\boldsymbol{\psi}_i, \quad \boldsymbol{x} \in E. \tag{25}$$

Note that $\tilde{\boldsymbol{\phi}}_i$ represents a 2×2 matrix, with non-zero off diagonal entries. This allows for a mixed interpolation of the rotation components (Bathe, 1996).

The standard approach to modeling a crack geometry is to explicitly mesh the line of discontinuity. In the next section, we describe how the standard approximation can be enriched with discontinuous functions to model fracture.

3.2. Enriched MITC approximation

Consider a mesh of MITC4 elements and an independent crack geometry as shown in Fig. 2. In the X-FEM framework, the crack is modeled by enriching the standard approximation with discontinuous and near-tip functions. In the following equations, we express the approximation in global form with a sum over all nodal degrees of freedom. The explicit dependence of the bilinear shape functions ϕ_i on the local parent coordinates $\boldsymbol{\xi}$ is also dropped for convenience.

The following enriched approximation is proposed for the plate displacements and section rotations in the bending terms:

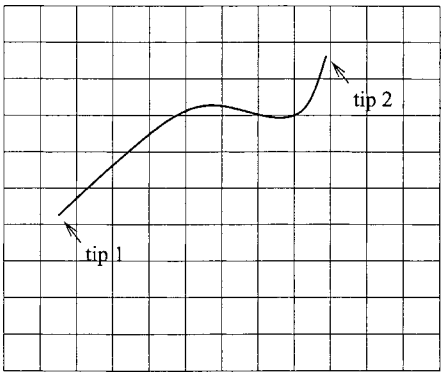

Fig. 2. An arbitrary crack placed on a mesh.

$$w^h(\boldsymbol{x}) = \sum_{i\in I} \phi_i(\boldsymbol{x}) w_i + \sum_{j\in J} \phi_j(\boldsymbol{x}) H(\boldsymbol{x}) b_j^w + \sum_{k\in K} \phi_k(\boldsymbol{x}) \left(\sum_{l=1}^{4} c_{kl}^w G_l(r,\theta) \right), \tag{26a}$$

$$\boldsymbol{\psi}^h(\boldsymbol{x}) = \sum_{i\in I} \phi_i(\boldsymbol{x}) \boldsymbol{\psi}_i + \sum_{j\in J} \phi_j(\boldsymbol{x}) H(\boldsymbol{x}) \boldsymbol{b}_j^\psi + \sum_{k\in K} \phi_k(\boldsymbol{x}) \left(\sum_{l=1}^{4} \boldsymbol{c}_{kl}^\psi F_l(r,\theta) \right). \tag{26b}$$

The section rotations in the shear terms are approximated by

$$\boldsymbol{\psi}^h(\boldsymbol{x}) = \sum_{i\in I} \tilde{\boldsymbol{\phi}}_i(\boldsymbol{x}) \boldsymbol{\psi}_i + \sum_{j\in J} \tilde{\boldsymbol{\phi}}_j(\boldsymbol{x}) H(\boldsymbol{x}) \boldsymbol{b}_j^\psi + \sum_{k\in K} \tilde{\boldsymbol{\phi}}_k(\boldsymbol{x}) \left(\sum_{l=1}^{4} \boldsymbol{c}_{kl}^\psi F_l(r,\theta) \right). \tag{27}$$

In the above equations, I is the set of all nodes, J, the set of nodes associated with the crack interior, and K, the set associated with the crack tip. The precise definitions of these sets is given later.

The above enriched approximation corresponds to applying the same reduction operator R in the MITC4 formulation, with the spaces $\mathscr{W}^h$, $\boldsymbol{\Psi}^h$, and Γ^h enriched with both discontinuous and near-tip fields. The extent to which the above approximation satisfies the criteria outlined in Brezzi et al. (1989) for an arbitrary crack and mesh geometry is an area for future research.

We now describe the construction of the discontinuous function $H(\boldsymbol{x})$ in two dimensions. This is a 'generalized Heaviside' function, in which the discontinuity is aligned with the surface Γ_d. The surface Γ_d is considered to be a curve parametrized by the curvilinear coordinate s, as in Fig. 3. Given a point $\boldsymbol{x}$ in the domain, we denote by $\boldsymbol{x}^*$ the closest point on Γ_d to $\boldsymbol{x}$. At $\boldsymbol{x}^*$, we construct the tangential and normal vector to the curve, $\boldsymbol{e}_s$ and $\boldsymbol{e}_n$, with the orientation of $\boldsymbol{e}_n$ taken such that $\boldsymbol{e}_s \times \boldsymbol{e}_n = \boldsymbol{e}_z$. The function $H(\boldsymbol{x})$ is then given by the sign of the scalar product $(\boldsymbol{x} - \boldsymbol{x}^*) \cdot \boldsymbol{e}_n$, i.e.

$$H(\boldsymbol{x}) = \begin{cases} 1 & \text{for } (\boldsymbol{x} - \boldsymbol{x}^*) \cdot \boldsymbol{e}_n > 0, \\ -1 & \text{for } (\boldsymbol{x} - \boldsymbol{x}^*) \cdot \boldsymbol{e}_n < 0. \end{cases} \tag{28}$$

In the case of a kinked crack as shown in Fig. 3(b), where no unique normal but a cone of normals is defined at $\boldsymbol{x}^*$, $H(\boldsymbol{x}) = 1$ if the vector $(\boldsymbol{x} - \boldsymbol{x}^*)$ belongs to the cone of normals at $\boldsymbol{x}^*$ and -1 otherwise.

The sets of near-tip functions G_l and F_l are expressed in terms of the local polar coordinates (r, θ) at each crack tip. They are derived from the sets of functions f_l and g_l which span the asymptotic near-tip fields for the section rotations and transverse displacements, respectively (see Section 4.1). We take G_l to be only those functions in g_l which are proportional to $r^{3/2}$. The set F_l is taken to be equivalent to f_l. These sets of

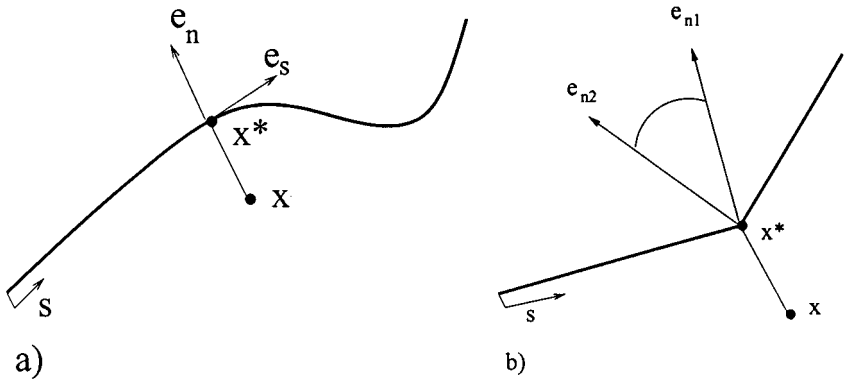

Fig. 3. Illustration of normal and tangential coordinates for a smooth crack (a) and for a crack with a kink (b). $\boldsymbol{x}^*$ is the closest point to $\boldsymbol{x}$ on the crack. In both of the above cases, the jump function H has value -1 at $\boldsymbol{x}$.

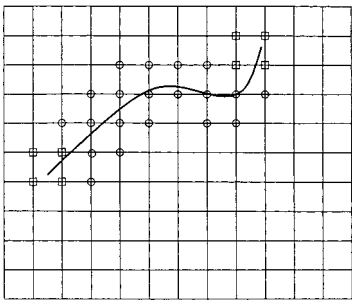

Fig. 4. Crack on a uniform mesh of MITC4 elements. The circled nodes are enriched by the jump function whereas the squared nodes are enriched by the crack tip functions.

near-tip functions were found to give the best overall results in terms of the performance with varying plate thickness and the accuracy of moment and shear force intensity factors. It bears emphasis that the near-tip discontinuity can be represented with other sets of functions, or even a single function which is discontinuous across the crack tip geometry (see Dolbow et al., 2000). In the context of linear elastic fracture mechanics, the incorporation of the exact near-tip asymptotic functions significantly improves the accuracy of the formulation. The studies presented in Section 5 provide further insight.

We now turn to the definitions of the sets J, K_1 and K_2. We shall denote by $\boldsymbol{x}_1$ and $\boldsymbol{x}_2$ the location of the crack tips 1 and 2 and by D the geometry of the crack discontinuity. The sets K_1 and K_2 consist of those nodes whose support closure contains crack tip 1 or 2, respectively. The set J is the set of nodes whose support is intersected by the crack and do not belong to K_1 or K_2. More precisely

$$K_1 = \{k \in I : \boldsymbol{x}_1 \in \overline{\omega}_k\}, \tag{29}$$

$$K_2 = \{k \in I : \boldsymbol{x}_2 \in \overline{\omega}_k\}, \tag{30}$$

$$J = \{j \in I : \omega_j \cap D \neq \emptyset, j \notin K_1, j \notin K_2\}, \tag{31}$$

where ω is the support of a node's shape function, with closure $\overline{\omega}$. Fig. 4 illustrates the sets J (circled nodes), K_1 (squared nodes near tip 1) and K_2 (squared nodes near tip 2) for a uniform mesh. In practice, the difference between the open set ω_j and its closure $\overline{\omega}_j$ in the definition of the set J is defined with a user-specified tolerance (see Dolbow et al., 2000).

3.3. Numerical integration

For elements cut by the crack and enriched with the jump function $H(\boldsymbol{x})$, it is necessary to make a modification to the element quadrature routines in order to accurately assemble the contribution to the Galerkin weak form on both sides of the discontinuity. As the crack is allowed to be arbitrarily oriented in an element, the use of standard Gauss quadrature may not adequately integrate the discontinuous field. If the integral of the function $H(\boldsymbol{x})$ is indistinguishable from that of a constant function, spurious singular modes can appear in the system of equations. In this section, we present the modifications made to the numerical integration scheme for elements cut by a crack.

The stiffness matrix is normally constructed with a loop over all elements, as the domain is approximated by

$$\overline{\Omega} = \bigcup_{e=1}^{m} \overline{\Omega}_e, \tag{32}$$

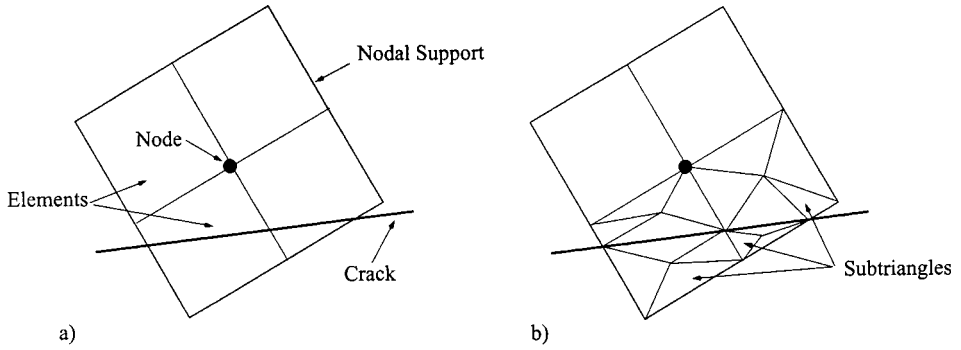

Fig. 5. (a) Nodal support cut by a crack. (b) The subtriangles associated with elements cut by the crack for node selection and the numerical integration of the weak form.

where m is the number of elements, and Ω_e, the element subdomain. For elements cut by a crack, we define the element subdomain to be a union of a set of subpolygons whose boundaries align with the crack geometry

$$\overline{\Omega}_e = \bigcup_{e=1}^{m_{es}} \overline{\Omega}_{es}, \tag{33}$$

where m_{es} denotes the number of subpolygons for the element.

The subtriangles implemented for nodal selection shown in Fig. 5 work well for integration across the discontinuity Γ_d. These subtriangles are also used to select nodes enriched with the discontinuous function $H(\boldsymbol{x})$, by calculating the percentage of a node's support above and below the crack. Simpler schemes, such as the trapezoids used by Fish (1989) and the formulation suggested in Dolbow (1999) may also perform adequately. The key feature is a consistent algorithm for nodal selection and enrichment. It is emphasized that the subpolygons are only necessary for integration purposes; no additional degrees of freedom are associated with their construction. In the integration of the weak form, the element loop is replaced by a loop over the subpolygons for those elements cut by the crack.

4. Extraction of mixed-mode intensity factors

In this section, we present the methodology for calculating the mixed-mode moment and shear force intensity factors for through cracks in Mindlin–Reissner plates. We begin by providing a brief summary of the pertinent quantities that arise when dealing with cracks in Mindlin–Reissner plates. The crack tip contour integrals which have previously been developed are reviewed, and we discuss why these integrals are not well suited for finite element analysis. This discussion motivates the derivation of a domain form of the interaction integral for Mindlin–Reissner plates.

4.1. Plate fracture mechanics

Consider the problem of a through crack in a plate as shown in Fig. 6, where for convenience we adopt a local polar coordinate system centered at the crack tip. As opposed to the stress intensity factors obtained in classical elasticity, in plate theory the quantities of interest are moment and shear force intensity factors. These are defined as

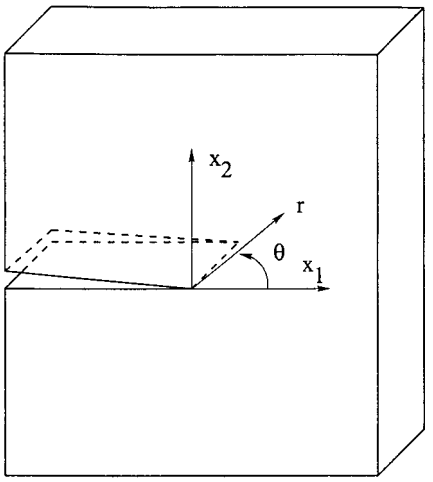

Fig. 6. Local polar coordinate system for through crack in plate.

$$K_1 = \lim_{r\to 0} \sqrt{2r} M_{22}(r,0), \quad K_2 = \lim_{r\to 0} \sqrt{2r} M_{12}(r,0), \quad K_3 = \lim_{r\to 0} \sqrt{2r} Q_2(r,0). \tag{34}$$

A link to the stress intensity factors of three-dimensional elasticity is made by considering the variation in stress components through the plate thickness. The bending stresses vary linearly through the plate thickness, while the transverse shear stresses vary parabolically. These considerations typically motivate the following relationships:

$$k_1(x_3) = \frac{12x_3}{t^3} K_1, \quad k_2(x_3) = \frac{12x_3}{t^3} K_2, \quad k_3(x_3) = \frac{3}{2t}\left[1 - \left(\frac{2x_3}{t}\right)^2\right] K_3. \tag{35}$$

The asymptotic displacement fields in Mindlin–Reissner plate theory can be found in Sosa and Eischen (1986) as a power series in $\sqrt{r}$. We list here only those terms proportional to $\sqrt{r}$ and $r^{3/2}$:

$$w = \frac{6\sqrt{2r}}{5t\mu} K_3 \sin\left(\frac{\theta}{2}\right) + \frac{6\sqrt{2}r^{3/2}K_1}{Et^3}\left[\frac{1}{3}(7+\nu)\cos\left(\frac{3\theta}{2}\right) - (1-\nu)\cos\left(\frac{\theta}{2}\right)\right] + \frac{6\sqrt{2}r^{3/2}K_2}{Et^3}\left[-\frac{1}{3}(5+3\nu)\sin\left(\frac{3\theta}{2}\right) + (1-\nu)\sin\left(\frac{\theta}{2}\right)\right] \tag{36a}$$

$$\psi_1 = \frac{6\sqrt{2r}K_1}{Et^3}\cos\left(\frac{\theta}{2}\right)[4-(1+\nu)(1+\cos(\theta))] + \frac{6\sqrt{2r}K_2}{Et^3}\sin\left(\frac{\theta}{2}\right)[4+(1+\nu)(1+\cos(\theta))] + \frac{6\sqrt{2}r^{3/2}K_3}{Et^3}\frac{8}{15}\left[-\sin\left(\frac{\theta}{2}\right) - (1+3\nu)\cos\left(\frac{\theta}{2}\right)\sin(\theta)\right]. \tag{36b}$$

$$\psi_2 = \frac{6\sqrt{2r}K_1}{Et^3}\left[4\sin\left(\frac{\theta}{2}\right) - (1+\nu)\left(\cos\left(\frac{\theta}{2}\right)\sin(\theta)\right)\right] + \frac{6\sqrt{2r}K_2}{Et^3}\left[-2\cos\left(\frac{\theta}{2}\right)(1-\nu) + (1+\nu)\sin\left(\frac{\theta}{2}\right)\sin(\theta)\right] + \frac{6\sqrt{2}r^{3/2}K_3}{Et^3}\frac{8}{15}\cos\left(\frac{\theta}{2}\right)[1+(1+3\nu)\cos(\theta)]. \tag{36c}$$

For the purposes of defining the near-tip enrichment functions in Section 3.2 for the plate theory, we consider only the terms proportional to $\sqrt{r}$ for the rotations ψ_1 and ψ_2. For the transverse displacement, we consider terms proportional to both $\sqrt{r}$ and $r^{3/2}$. With these restrictions, the above near-tip fields are contained in the span of the sets

$$w \in \{g_i(r,\theta)\}_{i=1}^{5}, \tag{37a}$$

$$\{\psi_1, \psi_2\} \in \{f_i(r,\theta)\}_{i=1}^{4}, \tag{37b}$$

where

$$\{g_I(r,\theta)\} \equiv \left\{\sqrt{r}\sin\left(\frac{\theta}{2}\right), r^{3/2}\sin\left(\frac{\theta}{2}\right), r^{3/2}\cos\left(\frac{\theta}{2}\right), r^{3/2}\sin\left(\frac{3\theta}{2}\right), r^{3/2}\cos\left(\frac{3\theta}{2}\right)\right\}, \tag{38a}$$

$$\{f_I(r,\theta)\} \equiv \left\{\sqrt{r}\sin\left(\frac{\theta}{2}\right), \sqrt{r}\cos\left(\frac{\theta}{2}\right), \sqrt{r}\sin\left(\frac{\theta}{2}\right)\sin(\theta), \sqrt{r}\cos\left(\frac{\theta}{2}\right)\sin(\theta)\right\}. \tag{38b}$$

The asymptotic near-tip moment and shear fields obtained from the displacement fields (34a)–(36c) are

$$M_{11} = \frac{K_1}{\sqrt{2r}}\cos\left(\frac{\theta}{2}\right)\left(1-\sin\left(\frac{\theta}{2}\right)\sin\left(\frac{3\theta}{2}\right)\right) - \frac{K_2}{\sqrt{2r}}\sin\left(\frac{\theta}{2}\right)\left(2+\cos\left(\frac{\theta}{2}\right)\cos\left(\frac{3\theta}{2}\right)\right), \tag{39a}$$

$$M_{22} = \frac{K_1}{\sqrt{2r}}\cos\left(\frac{\theta}{2}\right)\left(1-\sin\left(\frac{\theta}{2}\right)\sin\left(\frac{3\theta}{2}\right)\right) - \frac{K_2}{\sqrt{2r}}\sin\left(\frac{\theta}{2}\right)\cos\left(\frac{\theta}{2}\right)\cos\left(\frac{3\theta}{2}\right), \tag{39b}$$

$$M_{12} = \frac{K_1}{\sqrt{2r}}\sin\left(\frac{\theta}{2}\right)\cos\left(\frac{\theta}{2}\right)\cos\left(\frac{3\theta}{2}\right) + \frac{K_2}{\sqrt{2r}}\cos\left(\frac{\theta}{2}\right)\left(1-\sin\left(\frac{\theta}{2}\right)\sin\left(\frac{3\theta}{2}\right)\right), \tag{39c}$$

$$Q_1 = -\frac{K_3}{\sqrt{2r}}\sin\left(\frac{\theta}{2}\right), \tag{39d}$$

$$Q_2 = \frac{K_3}{\sqrt{2r}}\cos\left(\frac{\theta}{2}\right), \tag{39e}$$

where only the singular terms have been provided. We note that when the loading is purely K_1 or K_2, only the moments are singular at the crack tip. Similarly, when the loading is purely K_3, only the shears are singular.

4.2. Available crack-tip contour integrals

Several different domain and path-independent integrals have been developed for the extraction of mixed mode moment and shear force intensity factors in plates, see for example those derived in Sosa and Eischen (1986) or Sosa and Herrmann (1989). We summarize the results of these investigations here in order to motivate the developments which follow. In this section, we use indicial notation where the Greek indices (α, β) range over the values $1, 2$, and a comma denotes a partial derivative with respect to the following argument. We state the restrictions that the following development concerns the case when the crack-faces are traction free and there is no externally applied pressure on the plate.

The development of crack-tip contour integrals begins by considering the appropriate balance, or conservation law. Defining the strain energy in the plate as

$$W = \tfrac{1}{2}\left[M_{\alpha\beta}\psi_{\alpha,\beta} + Q_\beta(\psi_\beta + w_{,\beta})\right] \tag{40}$$

it can be shown that

$$W_{,k} - \left[M_{\alpha\beta}\psi_{\alpha,k} + Q_\beta w_{,k}\right]_{,\beta} = 0 \quad \text{for } k = 1,2 \tag{41}$$

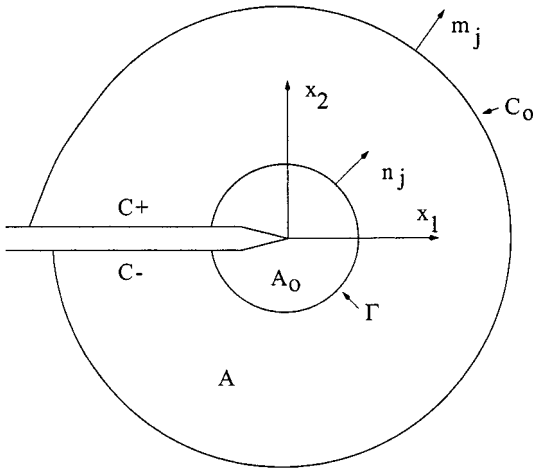

Fig. 7. Conventions at the crack tip. The domain A_0 is enclosed by Γ, while A is enclosed by Γ, C_+, C_-, and C_0.

using the plate equations (11a) and (11b), constitutive laws (13), and (14), and strain–displacement relations (4) and (5). The measures J_k are obtained by integrating the above expression over the domain A_0 enclosed by the contour Γ shown in Fig. 7. After applying the divergence theorem, we arrive at the following:

$$J_k = \oint_\Gamma \{W\delta_{k\beta} - \left[M_{\alpha\beta}\psi_{\alpha,k} + Q_\beta w_{,k}\right]\} n_\beta \, \mathrm{d}\Gamma. \tag{42}$$

The measures J_k vanish when the region enclosed by Γ does not contain a crack. In the present investigation, we are primarily concerned with the J_1 integral. When Γ is an open contour surrounding a crack tip, the J_1 integral is path independent and its magnitude is equivalent to the energy release rate corresponding to a unit crack advance in the x_1 direction.

The relationship between the energy release rate G and the moment and shear force intensity factors is determined as follows. The asymptotic fields (36a)–(36c) are substituted into the above integral, and a vanishingly small path enclosing the crack tip is considered. In the limit, only the singular terms $[\mathcal{O}(r^{-1})]$ contribute to the result

$$J_1 = G = \frac{12\pi}{Et^3}\left[K_1^2 + K_2^2\right] + \frac{\pi}{2k\mu t}K_3^2. \tag{43}$$

The calculation of J_1 in conjunction with the above equation is not sufficient to extract K_1, K_2, and K_3. While an analogous relationship can be derived for J_2, we are still left with only two equations for the three unknowns. To address this issue, Sosa and Herrmann (1989) separated the strain energy into bending and shear contributions as

$$W^{\mathrm{b}} = \tfrac{1}{2}\left[M_{\alpha\beta}\psi_{\alpha,\beta}\right], \qquad W^{\mathrm{s}} = \tfrac{1}{2}\left[Q_\beta(\psi_\beta + w_{,\beta})\right] \tag{44}$$

and derived the following integrals from the corresponding conservation laws:

$$J_k^{\mathrm{b}} = \int_\Gamma \{W^{\mathrm{b}}\delta_{k\beta} - M_{\alpha\beta}\psi_{\alpha,k}\} n_\beta \, \mathrm{d}\Gamma + \int_{A_0} Q_\beta \psi_{\beta,k} \mathrm{d}A, \tag{45a}$$

$$J_k^{\mathrm{s}} = \int_\Gamma \{W^{\mathrm{s}}\delta_{k\beta} - Q_\beta w_{,k}\} n_\beta \, \mathrm{d}\Gamma - \int_{A_0} Q_\beta \psi_{\beta,k} \mathrm{d}A. \tag{45b}$$

By substituting the near-tip fields into these expressions, the following relationships can be derived:

$$J_1^{\mathrm{b}} = \frac{12\pi}{Et^3}[K_1^2 + K_2^2], \tag{46a}$$

$$J_2^{\mathrm{b}} + J_2^{\mathrm{s}} = -\frac{24\pi}{Et^3}K_1K_2, \tag{46b}$$

$$J_1^{\mathrm{s}} = \frac{\pi}{2k\mu t}K_3^2. \tag{46c}$$

While the magnitude of K_3 can certainly be determined from Eq. (46c) above, we cannot determine its sign. Furthermore, the two Eqs. (46a) and (46b) are generally insufficient to separate K_1 and K_2. A quadratic equation results, and the two roots are indistinguishable. While both the sign of K_3 and the separation of K_1 and K_2 may be determined by additionally examining the form of the near-tip fields, this process is fairly cumbersome and does not lend itself to the automatic simulation of crack growth. An additional concern involves the numerical calculation of the contour integrals (45a) and (45b) in a finite element context. When the plate displacements are approximated with $C^0(\Omega)$ continuous shape functions, the moments $\boldsymbol{M}$ and shears $\boldsymbol{Q}$ will not be continuous across element boundaries on the contour Γ. This issue is typically addressed by using a 'smoothing' technique such as that suggested in Hinton and Campbell (1974). In the sections which follow, we illustrate how the development of the domain form of an interaction integral for plates circumvents all of the aforementioned difficulties.

4.3. The interaction integral

A particularly convenient method for extracting mixed-mode stress intensity factors is the interaction energy integral approach. Yau et al. (1980) and Shih and Asaro (1988) have employed interaction energy integrals to evaluate mixed-mode stress intensity factors in two-dimensional plane problems. In the present investigation, the interaction energy integrals are developed for extracting mixed-mode moment and shear force intensity factors in Mindlin–Reissner plates.

To derive the interaction integral, we begin by considering two states of field quantities: the present state $(\boldsymbol{M}, \boldsymbol{Q}, \psi, w)$, and an auxiliary state characterized by $(\boldsymbol{M}^{\mathrm{aux}}, \boldsymbol{Q}^{\mathrm{aux}}, \psi^{\mathrm{aux}}, w^{\mathrm{aux}})$. The J_1 integral for the sum of the two states is given by

$$J_1^{\mathrm{sum}} = \oint_\Gamma \{W^{\mathrm{sum}}\delta_{1\beta} - [(M_{\alpha\beta} + M_{\alpha\beta}^{\mathrm{aux}})(\psi_{\alpha,1} + \psi_{\alpha,1}^{\mathrm{aux}}) + (Q_\beta + Q_\beta^{\mathrm{aux}})(w_{,1} + w_{,1}^{\mathrm{aux}})]\}n_\beta \,\mathrm{d}\Gamma, \tag{47}$$

where

$$W^{\mathrm{sum}} = \tfrac{1}{2}\big[(\boldsymbol{M} + \boldsymbol{M}^{\mathrm{aux}}) : (\boldsymbol{\epsilon}_{\mathrm{b}} + \boldsymbol{\epsilon}_{\mathrm{b}}^{\mathrm{aux}}) + (\boldsymbol{Q} + \boldsymbol{Q}^{\mathrm{aux}}) \cdot (\boldsymbol{\epsilon}_{\mathrm{s}} + \boldsymbol{\epsilon}_{\mathrm{s}}^{\mathrm{aux}})\big]. \tag{48}$$

Expanding and rearranging terms gives

$$J_1^{\mathrm{sum}} = J_1 + J_1^{\mathrm{aux}} + I, \tag{49}$$

where I is the interaction integral given by

$$I = \oint_\Gamma \{W^{\mathrm{int}}\delta_{1\beta} - [M_{\alpha\beta}\psi_{\alpha,1}^{\mathrm{aux}} + M_{\alpha\beta}^{\mathrm{aux}}\psi_{\alpha,1} + Q_\beta w_{,1}^{\mathrm{aux}} + Q_\beta^{\mathrm{aux}} w_{,1}]\}n_\beta \,\mathrm{d}\Gamma \tag{50}$$

and W^{int} is the interaction strain energy

$$W^{\mathrm{int}} = \boldsymbol{M} : \boldsymbol{\epsilon}_{\mathrm{b}}^{\mathrm{aux}} + \boldsymbol{Q} \cdot \boldsymbol{\epsilon}_{\mathrm{s}}^{\mathrm{aux}} = \boldsymbol{M}^{\mathrm{aux}} : \boldsymbol{\epsilon}_{\mathrm{b}} + \boldsymbol{Q}^{\mathrm{aux}} \cdot \boldsymbol{\epsilon}_{\mathrm{s}}. \tag{51}$$

In a similar manner, the energy release rate corresponding to the sum of the present state and the auxiliary state is given by

$$G^{\text{sum}} = \frac{12\pi}{Et^3}\left[(K_1 + K_1^{\text{aux}})^2 + (K_2 + K_2^{\text{aux}})^2\right] + \frac{6\pi}{10\mu t}(K_3 + K_3^{\text{aux}})^2. \tag{52}$$

Upon rearranging terms we obtain

$$G^{\text{sum}} = J_1 + J_1^{\text{aux}} + \frac{24\pi}{Et^3}\left[K_1 K_1^{\text{aux}} + K_2 K_2^{\text{aux}}\right] + \frac{12\pi}{10\mu t} K_3 K_3^{\text{aux}}. \tag{53}$$

By equating J^{sum} in Eq. (49) with G^{sum}, we arrive at the following relationship:

$$I = \frac{24\pi}{Et^3}\left[K_1 K_1^{\text{aux}} + K_2 K_2^{\text{aux}}\right] + \frac{12\pi}{10\mu t} K_3 K_3^{\text{aux}}. \tag{54}$$

The auxiliary state is set to the leading order terms in the expressions for the exact near-tip fields (36a)–(36c) and (39a)–(39e). For the near-tip displacements, only those terms proportional to $\sqrt{r}$ are taken. The auxiliary strains are determined from Eqs. (39a)–(39e) and inverting the constitutive relationships (13) and (14). The process of evaluating the mixed-mode intensity factors involves making a judicious choice of the auxiliary moment and shear force intensity factors, and then evaluating the interaction energy integral (50). For example, to extract K_1, we set $K_1^{\text{aux}} = 1$, $K_2^{\text{aux}} = 0$, $K_3^{\text{aux}} = 0$, from which it follows from the above that

$$K_1 = \frac{Et^3}{24\pi} I. \tag{55}$$

The moment and shear force intensity factors K_2 and K_3 are extracted in a similar fashion. In order to numerically evaluate the interaction integral, it is advantageous to recast the contour integrals in their equivalent domain forms which are developed in the following section.

4.4. Domain form of the interaction integral

In this section, we illustrate the use of a weight function q to recast the line integrals developed in the previous section into their equivalent domain form. The domain forms are particularly well suited for use with finite elements, as the same quadrature points used for the construction of the bilinear form can be used to calculate the domain integral. Additional quadrature points or the use of a smoothing procedure are not required.

We begin with the contour integral presented in the previous section (Eq. (50)). Consider the simply connected curve $C = C_0 + C_+ + C_- + \Gamma$ as shown in Fig. 7. Following Moran and Shih (1987), we now introduce a weight function q which is sufficiently smooth in the area A enclosed by C, and is defined on the surfaces as

$$q = \begin{cases} 1 & \text{on } \Gamma \\ 0 & \text{on } C_0 \end{cases} \tag{56}$$

We then use this function to rewrite Eq. (50) as

$$\begin{aligned} I = \oint_C \Big\{ & - W^{\text{int}}\delta_{1\beta} + \left[M_{\alpha\beta}\psi_{\alpha,1}^{\text{aux}} + M_{\alpha\beta}^{\text{aux}}\psi_{\alpha,1} + Q_\beta w_{,1}^{\text{aux}} + Q_\beta^{\text{aux}} w_{,1}\right]\Big\} m_\beta q \, \mathrm{d}C \\ & - \int_{C_+ + C_-} \left[M_{\alpha 2}\psi_{\alpha,1}^{\text{aux}} + M_{\alpha 2}^{\text{aux}}\psi_{\alpha,1} + Q_2 w_{,1}^{\text{aux}} + Q_2^{\text{aux}} w_{,1}\right] m_2 q \, \mathrm{d}C, \end{aligned} \tag{57}$$

where we have used $m_i = n_i$ on C_0, $m_i = -n_i$ on Γ, and $m_1 = 0$, $m_2 = \pm 1$ on the crack faces. The last integral above vanishes for traction free crack faces. Applying the divergence theorem to the integral over A, we obtain

$$I = \int_A \left\{ \left[M_{\alpha\beta}\psi^{\text{aux}}_{\alpha,1} + M^{\text{aux}}_{\alpha\beta}\psi_{\alpha,1} + Q_\beta w^{\text{aux}}_{,1} + Q^{\text{aux}}_\beta w_{,1} \right] - W^{\text{int}}\delta_{1\beta} \right\} q_{,\beta}\, \mathrm{d}A$$
$$+ \int_A \left\{ \left[M_{\alpha\beta}\psi^{\text{aux}}_{\alpha,1} + M^{\text{aux}}_{\alpha\beta}\psi_{\alpha,1} + Q_\beta w^{\text{aux}}_{,1} + Q^{\text{aux}}_\beta w_{,1} \right] - W^{\text{int}}\delta_{1\beta} \right\}_{,\beta} q\, \mathrm{d}A. \tag{58}$$

The integrand in the second integral above needs to be examined in more detail. If the auxiliary fields satisfy the strain–displacement equations (4) and (5), the constitutive equations (13) and (14), and the equilibrium equations (11a) and (11b), then this integrand will vanish. When the auxiliary fields are chosen to be the leading order terms in r, however, either the equilibrium equations or the strain–displacement relationships will not be satisfied exactly. These conditions are similar to those studied in Gosz et al. (1998), where the auxiliary fields did not satisfy certain governing equations due to the curvature of the three-dimensional crack front. Consider the present conditions when the auxiliary fields correspond to a pure K_1 state. We have from Eqs. (39a)–(39e) that

$$\boldsymbol{Q}^{\text{aux}} = 0, \qquad \boldsymbol{\epsilon}^{\text{aux}}_{\text{s}} = 0 \tag{59}$$

and yet from Eqs. (36a)–(36c) the section rotations are non-zero, and so the strain–displacement relationship (5) is not satisfied. A similar situation arises when the auxiliary fields correspond to a pure K_2 state, and when the case is pure K_3 we have

$$\boldsymbol{M}^{\text{aux}} = 0, \qquad \nabla \cdot \boldsymbol{M}^{\text{aux}} = 0 \tag{60}$$

and yet the auxiliary shears are non-zero and so the equilibrium equations are not satisfied.

After a good deal of algebraic manipulations, the appropriate cancellations can be made to reduce Eq. (58) to the following domain form of the interaction integral:

$$I = \int_A \left\{ \left[M_{\alpha\beta}\psi^{\text{aux}}_{\alpha,1} + M^{\text{aux}}_{\alpha\beta}\psi_{\alpha,1} + Q_\beta w^{\text{aux}}_{,1} + Q^{\text{aux}}_\beta w_{,1} \right] - W^{\text{int}}\delta_{1\beta} \right\} q_{,\beta}\, \mathrm{d}A$$
$$+ \int_A \left\{ \left(M^{\text{aux}}_{\alpha\beta,\beta} - Q^{\text{aux}}_\alpha \right)\psi_{\alpha,1} + Q_\alpha \left(w^{\text{aux}}_{,\alpha 1} + \psi^{\text{aux}}_{\alpha,1} - \epsilon^{\text{aux}}_{\text{s}\,\alpha,1} \right) \right\} q\, \mathrm{d}A. \tag{61}$$

We remark that it is necessary to include the terms in the second integral to preserve the domain independence of the measure number I.

The above integral can be reduced depending on whether the quantity of interest is K_1, K_2, or K_3, as certain terms in the auxiliary fields vanish for each case. For example, for K_1 and K_2 the integral takes the form

$$I = \int_A \left\{ \left[M_{\alpha\beta}\psi^{\text{aux}}_{\alpha,1} + M^{\text{aux}}_{\alpha\beta}\psi_{\alpha,1} \right] - W^{\text{int}}\delta_{1\beta} \right\} q_{,\beta}\, \mathrm{d}A + \int_A (Q_\alpha \psi^{\text{aux}}_{\alpha,1}) q\, \mathrm{d}A, \tag{62}$$

whereas for K_3 the integral reads

$$I = \int_A \left\{ \left[Q_\beta w^{\text{aux}}_{,1} + Q^{\text{aux}}_\beta w_{,1} \right] - W^{\text{int}}\delta_{1\beta} \right\} q_{,\beta}\, \mathrm{d}A - \int_A (Q^{\text{aux}}_\alpha \psi_{\alpha,1}) q\, \mathrm{d}A. \tag{63}$$

It is noted that the above forms are similar to the bending and shear integrals (45a) and (45b) presented earlier. In fact, the above forms can also be derived by considering Eqs. (45a) and (45b) for the sum of two states, and then performing the same manipulations presented in this section.

Finally, if the auxiliary state variables are set to the present variables in the interaction integral, we recover the domain form of the J_1 integral for plates. This is given by

$$J_1 = \int_A \left\{ \left[M_{\alpha\beta}\psi_{\alpha,1} + Q_\beta w_{,1} \right] - W\delta_{1\beta} \right\} q_{1,\beta}\, \mathrm{d}A - \int_{C_+ + C_-} \left[M_{\alpha 2}\psi_{\alpha,1} + Q_2 w_{,1} \right] m_2 q_1\, \mathrm{d}C. \tag{64}$$

When the loading is known to be purely K_1, the above equation can be used in conjunction with Eq. (43) to calculate the moment intensity factor.

The proceeding development of a domain form of the interaction integral can be readily extended to other formulations, such as the Kirchhoff plate model. In addition, the incorporation of pressure loads and tractions on the crack faces does not place any restrictions on the formulation. The additional external forces simply enter into the equations in the form of surface and contour integrals (see Moran and Shih, 1987).

In the numerical examples given in the next section, the domain A is set from the collection of elements about the crack tip. Using a local characteristic length h_{local}, the domain is set to be all elements within a ball of radius r_{d} from the crack tip. We have used $r_{\text{d}} = 2h_{\text{local}}$. The weight function q takes a value of unity for all nodes within r_{d}, and zero on the outer contour. See Moës et al., 1999 for details.

5. Numerical examples

In this section, we present some examples using the extended MITC4 plate formulation. We first examine the accuracy of the method as a function of plate thickness for a benchmark problem, and then present a more general example. Throughout this section, the material properties are assumed to be isotropic with Young's modulus $E = 200$ GPa and Poisson's ratio $\nu = 0.3$.

5.1. Benchmark problem

As a benchmark problem we consider a through crack in an infinite plate subjected to a far-field moment M_0. The crack is oriented at an angle β with respect to the x_1 axis as shown in Fig. 8. Accurate calculations were carried out by Joseph and Erdogan (1991) for various plate thicknesses for $\beta = 0^\circ$. In this configuration, the loading is purely mode I, and the domain form of the J-integral for plates (64) is used in conjunction with Eq. (43) to determine the moment intensity factor K_I. We also take advantage of the symmetry about the x_2 axis (when $\beta = 0$) and model only one-half of the plate with finite elements. To approximate the infinite plate, the plate width W is taken to be 20 times the half crack length a. The crack length is taken to be $2a = 1.0$ for the results presented in this study .

Fig. 9 shows the normalized K_I for four discretizations, two with enrichment and two without. The lower curve corresponds to a standard MITC4 approximation, and the values for K_I are within 5% of the exact

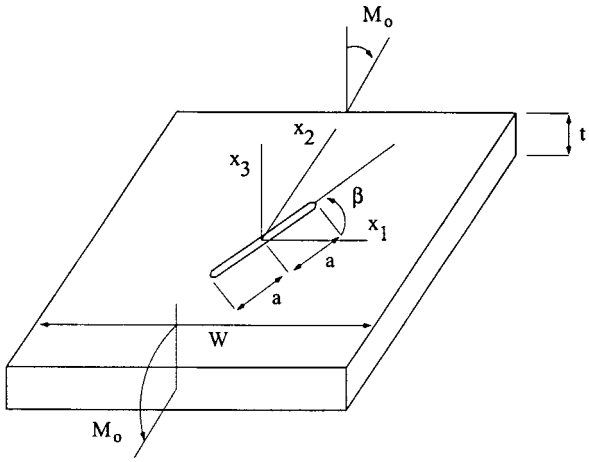

Fig. 8. Loading configuration for bending of cracked plate.

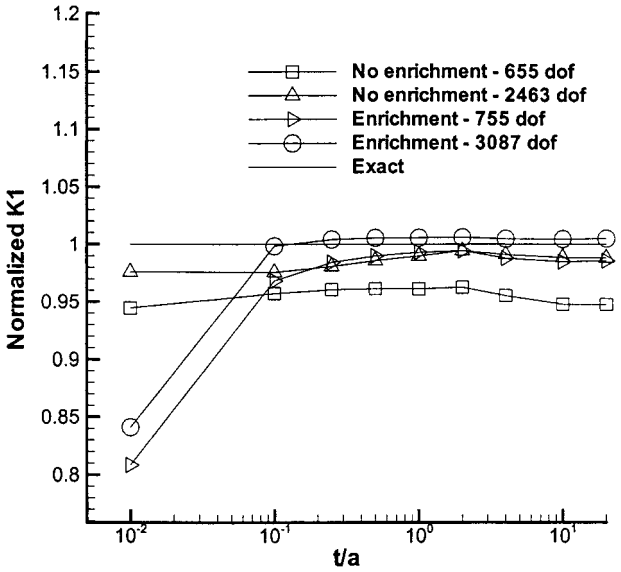

Fig. 9. Normalized moment intensity factors for varying plate thickness.

for the entire range of plate thicknesses. These values are improved when the mesh is refined for a total of 2463 degrees of freedom as shown. We observe that the solution obtained with the enriched approximation and only 755 degrees of freedom is as accurate as the standard approximation with 2463 degrees of freedom. The last curve for the enriched case with 3087 degrees of freedom exhibits less than 1% error. An exception concerns both enriched solutions when the normalized thickness $t/a = 0.01$, where a significant decrease in accuracy is observed. This deviation may be attributed to the onset of shear locking for the enriched approximation. We note that this occurs only for very thin plates ($t/W = 1/2000$), and that the calculated moment intensity factor K_1 for $t/a = 0.1$ is within 3% of the limiting value of 0.4439. This is illustrated in Fig. 10 where the moment intensity factor is not normalized.

Additional moment intensity factors are calculated for a finite plate as a function of crack length for various plate thicknesses. The geometry of the plate is taken to be the same as in the previous example, and the results are compared to those given in Boduroglu and Erdogan, 1983. In this study, the mesh does not model the crack discontinuity; the jump in the rotations and transverse displacement is created entirely with enrichment. Table 1 gives the results for four different width to thickness ratios for the case when the plate is modeled with 1424 MITC4 elements. These results show excellent correlation for the cases when $t = w/4$ and $t = w/8$, in which the maximum error is 1.2%. For the remaining cases the maximum difference between the numerical solutions and those given in Boduroglu and Erdogan (1983) is 9.4%. We remark that the results given in Boduroglu and Erdogan (1983) are not as reliable as those found in Joseph and Erdogan (1991). In the latter, the moment intensity factors are shown to be significantly greater than the classical results Sih (1977) as the thickness $t \to 0$. The results shown in Table 1 are consistent with these findings.

5.2. Angled center crack

We now present results for the moment and shear force intensity factors as a function of the angle β for the geometry of Fig. 8. These results serve to illustrate the versatility of the present formulation, as well as the validity of the interaction integral derived in Section 4.4.

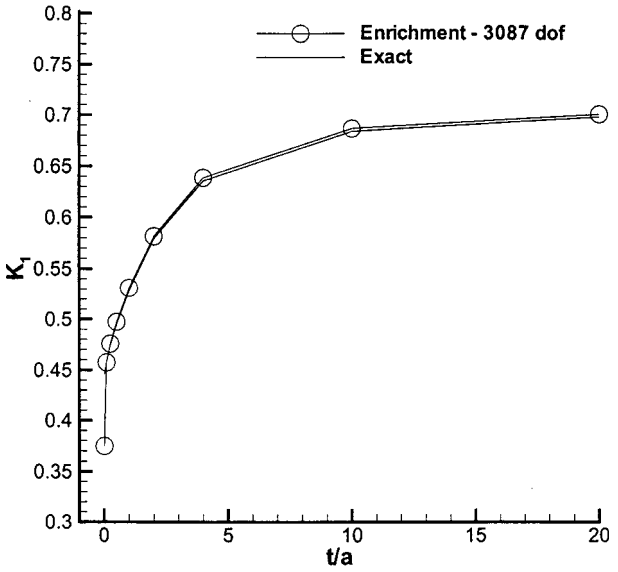

Fig. 10. Moment intensity factors for varying plate thickness.

Table 1
Normalized K_I values for finite plate

$t = w/4$		$t = w/8$		$t = w/12$		$t = w/16$	
a/w	K_I/K_I^{ref}	a/w	K_I/K_I^{ref}	a/w	K_I/K_I^{ref}	a/w	K_I/K_I^{ref}
0.025	0.988	0.025	0.989	0.0333	1.067	0.0250	1.077
0.05	0.992	0.050	0.993	0.0500	1.052	0.0375	1.090
0.10	0.997	0.075	0.995	0.0667	1.069	0.0500	1.094
0.20	1.000	0.100	0.996	0.0833	1.070	0.0625	1.092
0.25	0.999	0.125	0.997	0.1667	1.054	0.1250	1.072
0.333	1.013	0.250	0.998	0.3333	1.057	0.2500	1.062

We consider the case of a relatively thick plate, by taking $t/a = 2$. The exact solution for the infinite plate is given in Sih (1977) as

$$K_1 = \Phi(1) M_0 \sqrt{a} \cos^2 \beta, \tag{65a}$$

$$K_2 = \Psi(1) M_0 \sqrt{a} \cos \beta \sin \beta, \tag{65b}$$

$$K_3 = -\frac{\sqrt{10}}{(1+\nu)t} \Omega(1) M_o \sqrt{a} \cos \beta \sin \beta, \tag{65c}$$

where the functions $\Phi(1)$, $\Psi(1)$, and $\Omega(1)$ are computed numerically from integral equations. When $t/a = 2$, these are approximately 0.82, 0.68 and 0.06, respectively. We remark that Joseph and Erdogan (1991) have questioned the validity of the above relationships for thinner plates.

We present results as a function of β for two situations. In the first case, a portion of the mesh is rotated such that the element edges align with the geometry of the crack. A typical mesh of 1920 MITC4 elements is shown in Fig. 11. In the second case, the same number of elements is used but the the mesh is not rotated and the crack cuts across element boundaries. In all configurations, the plate displacements are discretized with the enriched MITC4 approximation (26a) and (26b).

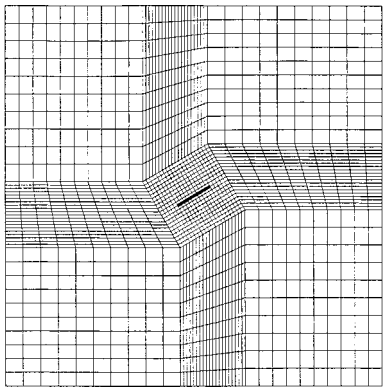

Fig. 11. Mesh with typical rotated center section. The crack geometry is shown in bold.

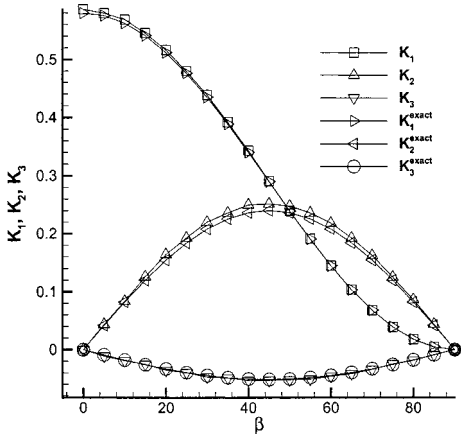

Fig. 12. Normalized moment and shear force intensity factors for center crack at angle β. The crack is aligned with the mesh.

Fig. 12 shows the results when the crack aligns with the mesh. The numerical results show good correlation with the exact values for the full range of β. The results for a fixed mesh are shown in Fig. 13. While the agreement between the numerical and the exact results for K_1 and K_2 is acceptable, there is substantial deviation in K_3. From Eqs. (39a)–(39e), we observe that there is a strong relationship between the shear force intensity factor and the shear fields $\boldsymbol{Q}$. For pure K_3 loading, only the shears Q_1 and Q_2 are singular. As the approximation for the shear is also modified by the MITC formulation to avoid locking, we can conclude from these studies that a crack cutting across element boundaries adversely affects this approximation. An improvement in the results is achievable with finer discretization, and Fig. 14 shows the results using a mesh of 4080 MITC4 elements.

6. Summary and concluding remarks

In this paper, a new formulation for modeling cracks in plates in the Mindlin–Reissner framework has been presented. The form of the enriched approximation is similar to that in Moës et al. (1999), with different sets of near-tip functions for the rotations and transverse displacement. In order to extract the

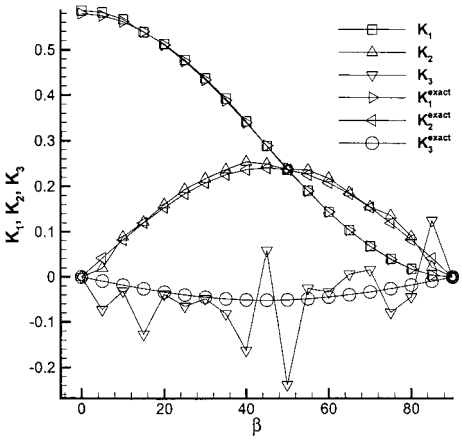

Fig. 13. Normalized moment and shear force intensity factors for center crack at angle β. The crack is not aligned with the mesh.

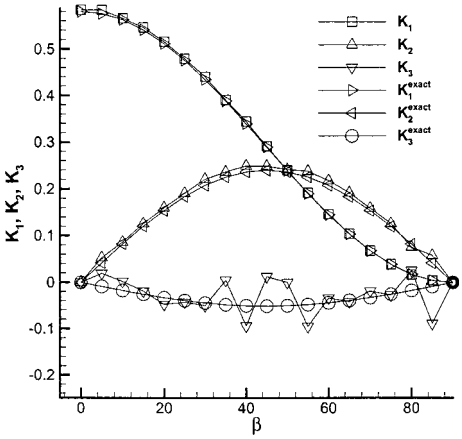

Fig. 14. Normalized moment and shear force intensity factors for center crack at angle β. The crack is not aligned with the mesh of 4080 MITC4 elements.

mixed-mode intensity factors, appropriate domain forms of the interaction integral were derived. A key component to the success of the domain integrals is the incorporation of terms which arise from the failure of the auxiliary fields to satisfy the equilibrium and strain–displacement equations. Several benchmark problems illustrated good performance for the formulation over a range of plate thicknesses. Some adverse effects of the enrichment were noticed in the calculation of the shear force intensity factor when the crack cut across element boundaries.

Further studies are required to determine the extent to which the present enriched formulation avoids shear locking. The selection of approximating spaces which do not exhibit shear locking are usually formulated in terms of the local polynomial spaces on the element level. A difficulty with the enriched basis functions is that they are constructed using both the element and crack geometries, as opposed to just a map with a parent element. It is precisely this construction which gives the enriched formulation the flexibility to model cracks which are not oriented with the mesh. The form of the enriched approximation is flexible in the selection of the near-tip functions, and some modifications to the generalized Heaviside

function can also be envisaged. It may therefore be possible to construct an enriched approximation which completely avoids shear locking.

The present formulation offers significant promise to model crack growth in plates and shells. As the crack geometry can be represented independently of the mesh, it is not necessary to remesh the domain at each step in the simulation. Good correlation with experimental results has been obtained using the X-FEM in two-dimensional plane strain calculations Dolbow (1999). With regards to modeling crack growth in plates, all that is required is a suitable crack growth law. While several different crack growth laws have been developed for plates subjected to in-plane loads, little attention has focused on the three-dimensional effects resulting from bending loads. The development of a suitable crack growth law for plates and comparison to experimental results is therefore the focus of current research.

Acknowledgements

The support of the Office of Naval Research and Army Research Office, to Northwestern University, is gratefully acknowledged. The authors are grateful for the support provided by the DOE Computational Science Graduate Fellowship program to John Dolbow. The authors are also thankful to Professor Manil Suri for several helpful conversations on shear locking.

References

Babuška, I., Rosenzweig, M., 1972. A finite element scheme for domains with corners. Numerical Mathematics 20, 1–21.

Bathe, K., 1996. Finite Element Procedures. Prentice Hall, Englewood Cliffs, New Jersey.

Bathe, K., Bucalem, M., Brezzi, F., 1990. Displacement and stress convergence of our MITC plate bending elements. Engineering Computations 7, 291–302.

Belytschko, T., Black, T., 1999. Elastic crack growth in finite elements with minimal remeshing. International Journal of Numerical Methods in Engineering 45 (5), 601–620.

Boduroglu, H., Erdogan, F., 1983. Internal and edge cracks in a plate of finite width under bending. Journal of Applied Mechanics 50, 621–628.

Brezzi, F., Bathe, K., Fortin, M., 1989. Mixed-interpolated elements for Reissner–Mindlin plates. International Journal of Numerical Methods in Engineering 28, 1787–1801.

Dolbow, J., 1999. An extended finite element method with discontinuous enrichment for applied mechanics. Northwestern University.

Dolbow, J., Moës, N., Belytschko, T., 2000. Discontinuous enrichment in finite elements with a partition of unity method. Finite Elements in Analysis and Design, in press.

Duarte, C., Oden, J., 1995. Hp clouds – a meshless method to solve boundary-value problems. Techinical report, TICAM.

Fish, J., 1989. Finite Element Method for Localization Analysis, Ph.D. Thesis, Northwestern University.

Gosz, M., Dolbow, J., Moran, B., 1998. Domain integral formulation for stress intensity factor computation along curved three-dimensional interface cracks. International Journal of Solids and Structures 35, 1763–1783.

Grisvard, P., 1985. Elliptic Problems in Nonsmooth Domains. Pitman, Boston.

Hinton, E., Campbell, J.S., 1974. Local and global smoothing of discontinuous finite element functions using a least squares method. International Journal of Numerical Methods in Engineering 8, 461–480.

Hughes, T., Tezduyar, T., 1981. Finite elements based upon Mindlin plate theory with particular reference to the four-node bilinear isoparametric element. Journal of Applied Mechanics 48, 587–596.

Hui, C., Zehnder, T., 1993. A theory for the fracture of thin plates subjected to bending and twisting moments. International Journal of Fracture 61, 211–229.

Joseph, P., Erdogan, F., 1991. Bending of a thin Reissner plate with a through crack. Journal of Applied Mechanics 58, 842–846.

Knowles, J., Wang, N., 1960. On the bending of an elastic plate containing a crack. J. Math. Phys. 39 (4), 223–236.

Melenk, J.M., Babuška, I., 1996. The partition of unity method: Basic theory and applications. Computer Methods in Applied Mechanics and Engineering 39, 289–314.

Moës, N., Dolbow, J., Belytschko, T., 1999. A finite element method for crack growth without remeshing. International Journal of Numerical Methods in Engineering 46, 131–150.

Moran, B., Shih, C., 1987. Crack tip and associated domain integrals from momentum and energy balance. Engineering Fracture Mechanics 127, 615–642.

Pitkäranta, J., Suri, M., 1996. Design principles and error analysis for reduced-shear plate-bending finite elements. Numerische Mathematik 75, 223–266.

Pitkäranta, J., Suri, M., 2000. Upper and lower bounds for plate-bending finite elements. Numerische Mathematik 84, 611–648.

Potyondy, D., Wawrzynek, P., Ingraffea, A., 1995. Discrete crack growth analysis methodology for through cracks in pressurized fuselage structures. International Journal of Numerical Methods in Engineering 38, 1611–1633.

Shih, C., Asaro, R., 1988. Elastic–plastic analysis of cracks on bimaterial interfaces: part I – small scale yielding. Journal of Applied Mechanics 55, 299–316.

Sih, G., 1977. Mechanics of Fracture 3: Plates and Shells with Cracks. Noordhoff, The Netherlands.

Sosa, H., Eischen, J., 1986. Computation of stress intensity factors for plate bending via a path-independent integral. Engineering Fracture Mechanics 25 (4), 451–462.

Sosa, H., Herrmann, G., 1989. On invariant integrals in the analysis of cracked plates. International Journal of Fracture 40, 111–126.

Yau, J., Wang, S., Corten, H., 1980. A mixed-mode crack analysis of isotropic solids using conservation laws of elasticity. Journal of Applied Mechanics 47, 335–341.